COMPDYN 2011
3rd ECCOMAS Thematic Conference on
Computational Methods in Structural Dynamics and Earthquake Engineering
M. Papadrakakis, M. Fragiadakis, V. Plevris (eds.)
Corfu, Greece, 25-28 May 2011

DAMAGE EVOLUTION IN STEEL STRUCTURES UNDER SEISMIC EXCITATION

Sven Heinrich[1], **Ursula Kowalsky**[1], **Jana Velde**[1], **and Dieter Dinkler**[1]

[1]Institute for Structural Analysis
Technische Universität Braunschweig
Beethovenstr. 51, 38106 Braunschweig, Germany
e-mail: s.heinrich@tu-bs.de

Keywords: Continuum damage mechanics, isotropic hardening, kinematic hardening, softening, seismic excitation, structural analysis, global damage index

Abstract. *For the purpose of energy dissipation steel structures exposed to seismic loading intentionally experience inelastic material behavior. Experiments of mild construction steel have shown that the behavior of structural steel is highly sensitive to loading velocity. Under cyclic loading, the Bauschinger effect decreases the yield stress. In addition, the steel suffers from material damage if the material is subjected to inelastic deformations.*
Therefore, to evaluate the structural safety of steel structures in case of earthquakes, a more detailed description of the material behavior is inevitable. The proposed material model describes the evolution and distribution of inelastic strains and damage in steel structures under seismic excitation by means of a set of internal variables. The model takes into account viscoplastic material behavior, isotropic and kinematic hardening, ductile damage, and a nonlocal extension in the form of an implicit gradient formulation to overcome the phenomenon of strain localization. To determine the material model parameters, numerical results are compared with experiments under static and dynamic loading. In order to indicate the influence of the description of the material behavior on the respsonse of 3D structures subjected to seismic excitation different approaches for the material are used.

1 INTRODUCTION

Earthquakes are unpredictable disasters which can damage structures severely and therefore endanger human safety. Thus, building codes in periled regions have to include methods to verify this special loading. The European code EC 8 uses the linear response spectrum method to specify static forces which act on the structure. The response spectrum is determined for elastic material behavior and the verification does not differ from static load cases. Material-dependent energy dissipation is taken into account by decreasing the response spectrum, and therefore the load, by a factor. This is a simple practical approach which considers the material behavior in a very general way depending on the method of construction.

Moreover the EC 8 also permits nonlinear time-history computations, but demands precise material modelling to capture the energy dissipation. In order to predict the structural response to seismic loading the inelastic material behavior, that accounts for the dissipation of energy, needs to be described in detail. Along with inelastic deformations a deterioration of the material can be observed, which is referred to as damage. It evolves from voids in the microstructure and this microstructural damage, which is not visually detectable from the outside, can increase over time and finally lead to macrocracks and failure [1, 2]. This paper focuses on a method to predict even small damage with a high precision. For that purpose, a continuum damage model is developed in the framework of thermodynamics taking into account the evolution of the material behavior including phenomena like hardening, softening, and damage. Since softening and damage are always accompanied by localization of deformation in small process zones of undefined width, local damage models suffer from a dependency on the fineness of finite-element discretization. As a remedy an implicit gradient enhanced formulation for a non-local damage variable is introduced which includes an additional material-dependent parameter to affect the size of the process zone.

Applying the proposed model to a FE analysis of a structure provides the distribution of damage across the structure. Therefore, highly stressed regions can be identified, but it is not possible to evaluate the damage state of the structure in general which encourages the formulation of a scalar global damage index.

2 MATERIAL MODEL

For the designing of steel constructions linear elastic material behavior is generally considered. To increase the degree of utilization plastic material behavior can be taken into account through a plain linear elastic ideal plastic stress-strain relationship.

For static loads these assumptions are conservative. To compute the response of a structure excited by earthquakes this simplified description of the material behavior is insufficient.

2.1 Material behavior of mild construction steel

To reveal the material behavior of mild construction steel subjected to seismic loading, experiments have been conducted at the Technische Universität Braunschweig [3]. Figure 1 depicts the measured stress of a unaxial bar loaded by a strain record deduced from the north-south component of the 1995 Kobe earthquake. The characteristic yield stress occurs only for the first load path. Beginning with the first reverse loading hystereses develop which exhibit a continuous transition between the linear elastic and the nonlinear inelastic range. The hysteresis shape shows that the initiation of plastic deformations occurs earlier after load reversals. This phenomenon called Bauschinger effect can be taken into account by kinematic hardening. Repeated cyclic straining with strain amplitudes $> 6\%$ leads to cyclic increase of the yield

stress which can be described by isotropic hardening. Moreover, experiments have shown that the cyclic deformation behavior of mild steel is closely related to the inelastic strain amplitude history [4, 5]. In order to consider this fact, a strain memory surface is integrated into the model.

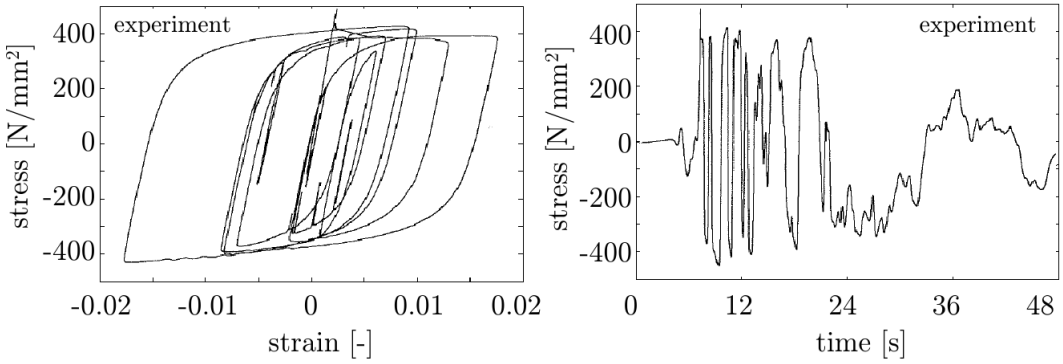

Figure 1: Hysteresis curves and development of stress of the Kobe earthquake obtained experimentally [3]

At he level of atoms inelastic deformations decrease the number of bonds which leads to material deterioration with an impairment of the elementary area of resistance. This damage is, in general, strongly anisotropic and can be observed as growing microvoids which eventually results in macroscopic cracks. For a low alloy steel Figure 2 shows the microscopic debonding of a notched specimen after cycling loading. The cross section is deteriorated although a macro-crack cannot be located yet. The existence of damage in mild steel is investigated for example in [7, 8].

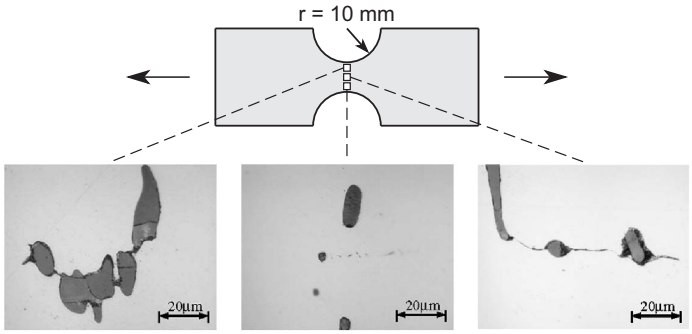

Figure 2: Metallographic section of a notched specimen after cyclic loading according to [6]

For the description of damage evolution a model is proposed which bases on the isotropic ductile damage model for monotonic loading presented in [9]. Modifications adjust the model to micromechanical observations under cyclic straining. The initiation of ductile damage is difficult to specify. Experiments have shown that nucleation of cavities does not occur below a certain amount of plastic strain. However, it is hard to determine this threshold so that a large variety of different proposals is available in literature. This work uses a threshold based on the equivalent plastic strain in order to capture the characteristics of mild construction steel. Since mild construction steel S 355 does not show pronounced damage in the form of a continuous reduction of the modulus of elasticity for cyclic loading with small strain amplitudes [10], the

model prohibits damage evolution below a certain amount of plastic strain. But ductile damage due to irregular large cyclic straining ist captured. The chosen criterion enables ductile damage evolution under large strains and thus provides a precise method in order to describe damage evolution under seismic loading.

2.2 Material equations

The mathematical description of the material behavior is achieved by a set of ordinary differential equations of first order with respect to time. The current state of the material is described by internal variables and related evolution equations, which can be derived from thermodynamics. The material equations contain isotropic nonlocal damage $\bar{D}$.

Assuming small strains, the total strain rate can be split up additively in an elastic and an inelastic part

$$\dot{\boldsymbol{\varepsilon}} = \dot{\boldsymbol{\varepsilon}}^{el} + \dot{\boldsymbol{\varepsilon}}^{in}. \tag{1}$$

The elastic strain rate is based on Hooke's law and contains an isotropic degradation of the modulus of elasticity by the damage variable $\bar{D}$ following the principle of energy equivalence [11]. Considering the influence of damage on stiffness under alternating tension and compression, it is assumed according to Lemaitre [12] that some but not every crack closes under compression so that the stiffness of the material under compression lies between the undamaged and the damaged stiffness. In order to define the compressive stiffness of damaged material a crack closure parameter h is introduced. Thus, effective stress and strain are defined differently for tension (+) and compression (-):

$$\tilde{\boldsymbol{\sigma}}^{+} = \frac{1}{1-D} \cdot \boldsymbol{\sigma}^{+} \quad , \quad \tilde{\boldsymbol{\varepsilon}}^{+} = (1-D) \cdot \boldsymbol{\varepsilon}^{+} \tag{2}$$

$$\tilde{\boldsymbol{\sigma}}^{-} = \frac{1}{1-Dh} \cdot \boldsymbol{\sigma}^{-} \quad , \quad \tilde{\boldsymbol{\varepsilon}}^{-} = (1-Dh) \cdot \boldsymbol{\varepsilon}^{-}. \tag{3}$$

For $h = 0$ the initial stiffness of the material is recovered and a value of $h = 1$ assumes that the stiffness under tension is on par with the stiffness under compression. Lemaitre proposes to use a value of $h = 0.2$. Figure 3 shows the characteristic development of the stiffness for cyclic loading if damage evolution for positive stress states is assumed.

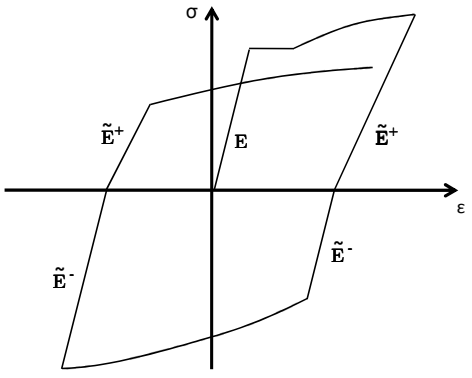

Figure 3: Stiffness under tenion and compression

The inelastic viscoplastic deformations are obtained following the approach by Chaboche and Rousselier [1, 2]. The over-stress σ_{ex}, that determines the onset of viscoplastic deformation,

corresponds to the yield function and results from a modified criterion based on Gurson [13] and Tvergaard and Needleman [14] with the first ($J_1(\boldsymbol{\sigma}_{eff}) = \frac{1}{3}tr(\boldsymbol{\sigma} - \mathbf{X})$) and the second ($J_2(\boldsymbol{\sigma}^d_{eff}) = \frac{1}{2}tr((\boldsymbol{\sigma} - \mathbf{X})^d \cdot (\boldsymbol{\sigma} - \mathbf{X})^d)$) invariant of the effective stress tensor $\boldsymbol{\sigma}_{eff} = \boldsymbol{\sigma} - \mathbf{X}$ and the effective stress deviator $\boldsymbol{\sigma}^d_{eff} = (\boldsymbol{\sigma} - \mathbf{X})^d$, respectively

$$\sigma_{ex} = \sigma_{eq} - \sigma_F - K = \frac{1}{1-\bar{D}}\sqrt{3J_2(\boldsymbol{\sigma}^d_{eff}) + \bar{D}J_1(\boldsymbol{\sigma}_{eff})^2} - \sigma_F - K. \tag{4}$$

The yield function considers isotropic hardening K and kinematic hardening $\mathbf{X}$ which appropriately describe inelastic behavior according to Chaboche and Rousselier in case of undamaged material by the v. Mises yield criterion.

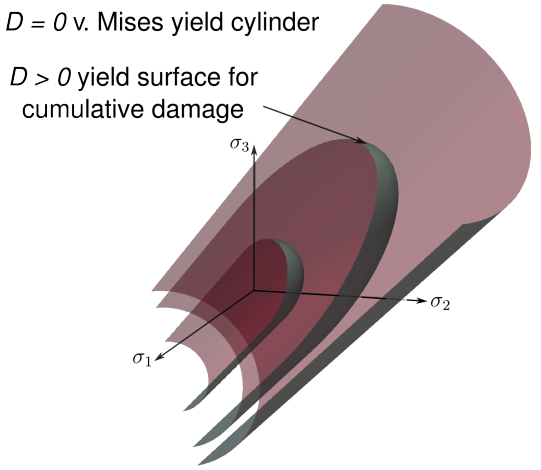

Figure 4: Yield surface

Figure 4 depicts the v. Mises yield cylinder for undamaged material and the contraction of the yield surface combined with a formation of caps at the ends of the yield cylinder due to damage. In case of damage, the yield function employs volumetric inelastic deformations and permits coupling of viscoplasticity and damage.

The initiation of damage is determined by a damage threshold surface which is defined via the equivalent positive plastic strain

$$\varepsilon^{in}_{eq} = \sqrt{\frac{2}{3}\left(\langle\varepsilon^{in}_{11}\rangle^2 + \langle\varepsilon^{in}_{22}\rangle^2 + \langle\varepsilon^{in}_{33}\rangle^2 + 2\langle\varepsilon^{in}_{12}\rangle^2 + 2\langle\varepsilon^{in}_{13}\rangle^2 + 2\langle\varepsilon^{in}_{23}\rangle^2\right)} \tag{5}$$

where the McAuley brackets omit negative strains and thus prohibit damage evolution under compression. The equivalent strain has to exceed the scalar damage threshold strain parameter ε^{in}_D for damage evolution

$$\begin{aligned} \varepsilon^{in}_{eq} - \varepsilon^{in}_D \leq 0 &\longrightarrow \dot{D} = 0 \\ > 0 &\longrightarrow \dot{D} \end{aligned} \tag{6}$$

While Pirondi and Bonora [15] propose that the damage threshold strain decreases under compression due to the presence of broken inclusions, the damage threshold strain here is assumed

to be constant.

In order to consider different damage evolution under tension and compression, the evolution of local ductile damage

$$\dot{D} = (c_1 + c_2 e^{-c_3 \frac{1}{(1-\bar{D})} p^+}) \frac{1}{(1-\bar{D})} \dot{p}^+ + c_4 (c_5 - \bar{D}) \left\langle tr \left(\frac{\partial \sigma_{ex}}{\partial \boldsymbol{\sigma}} \dot{p}^+ \right) \right\rangle \tag{7}$$

depends on a newly defined variable p^+ called active accumulated plastic strain based on [15]:

$$\dot{p}^+ = \dot{p} \left\langle \frac{J_1}{|J_1|} \right\rangle = \dot{\varepsilon}_0 \left\langle \frac{\sigma_{ex}}{\sigma_p} \right\rangle^n \left\langle \frac{J_1}{|J_1|} \right\rangle . \tag{8}$$

Thus, the evolution of ductile damage is enabled only if the first invariant of the stress tensor is positive. The two terms of the damage evolution equation (7) consider transient and saturation behavior in damage evolution as well as damage due to volumetric yielding and depend on the damage parameters c_1 - c_5.

The memory of the strain loading history is considered by a strain memory surface M, which depends on two variables $\boldsymbol{\beta}$ and q where $\boldsymbol{\beta}$ describes the displacement of the surface and q specifies its amplitude. Within this work, a maximum strain amplitude memory [4] is defined in the three-dimensional space as

$$M = \frac{2}{3} (\boldsymbol{\varepsilon}^{in} - \boldsymbol{\beta})(\boldsymbol{\varepsilon}^{in} - \boldsymbol{\beta}) - q^2 \leq 0 \tag{9}$$

with

$$\dot{\boldsymbol{\beta}} = 0.5 H(M)\ \dot{\boldsymbol{\varepsilon}}^{in}, \tag{10}$$

$$\dot{q} = 0.5 H(M)\ \mathbf{n}_F\ \mathbf{n}_M\ \dot{p}, \tag{11}$$

where $H(M)$ is the Heaviside function with $H(M) = 1$ if $M \geq 0$ and $H(M) = 0$ if $M < 0$, $\mathbf{n}_F$ is the normal to the yield surface, and $\mathbf{n}_M$ is the normal to the strain memory surface. A plastic strain state outside the current strain memory surface leads to the growth and adjustment of the variables $\boldsymbol{\beta}$ and q, while $\boldsymbol{\beta}$ and q remain constant for plastic strain states inside the memory surface. Thus, the inelastic strain amplitude variable q will not decrease and always remembers the maximum strain reached so far during loading.

Considering the influence of the strain memory surface on isotropic hardening, the saturation value of isotropic hardening Q becomes a function of the amplitude of the strain memory surface q. Within this work, the evolution rule of the saturation value of isotropic hardening Q is assumed to be linear.

As shown in Figure 5 the numerical results according to the proposed model match the measured stress, comparing Figure 1, very well. Solely the observed yield plateau cannot be described with the given model.

2.3 Non-local extension

The dissipation of energy concentrates on small areas of the structure called process zones. With the grave decrease of stiffness when reaching inelastic material behavior this causes high strain gradients. If the size of the process zone is not defined in a finite element computation the results of local damage models depend on the fineness of discretization. Reducing the element

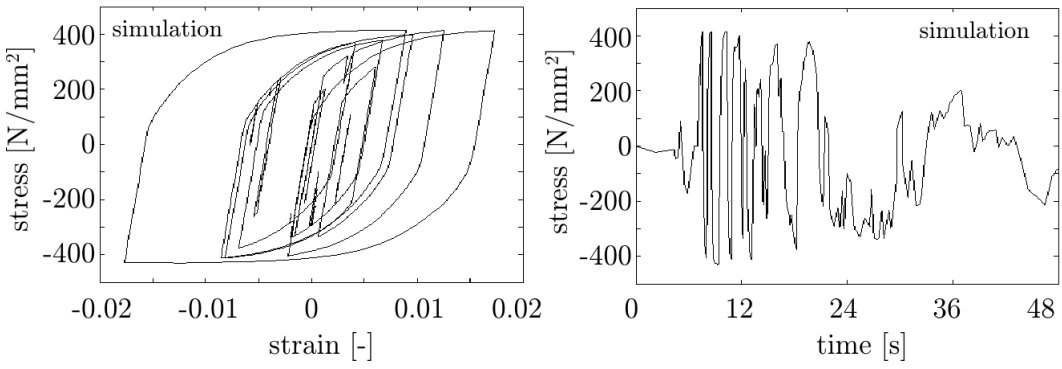

Figure 5: Hysteresis curves and development of stress of the Kobe earthquake obtained by numerical simulation

size leads to a decreasing process zone and less energy dissipated. It is obvious that for an evanescent volume and therefore inelastic material behavior without dissipation the description is physically incorrect and an extension to provide accurate results is needed. Mathematically, the problem becomes ill-posed since the differential equations lose their elliptic form and the acoustic tensor of the tangential stiffness tensor becomes singular [12, 16].

In order to determine the size of the process zone and to regularize the solution, the models need to be extended by a material-dependent internal length scale. An overview of the state of the art for different non-local extensions may be found in [17, 18]. Peerlings et al. [19] and Engelen et al. [20] show the derivation of models with gradients of internal variables from nonlocal integral models and differentiate between explicit and implicit gradient models.

This work examines the use of non-local implicit gradient models in 3D-FE structural analysis. By means of an additional gradient equation, non-local substitutes of the local variables can be obtained. Following the derivation of Engelen [20] and using gradients of the damage variables, the non-local damage variable $\bar{D}$ can be determined by the gradient equation

$$\bar{D} - l_c^2 \nabla^2 \bar{D} = D \tag{12}$$

with the local damage variable D for which its evolution equation is given with Eq. 7, the material-specific internal length l_c and the boundary condition $\nabla \bar{D} = 0$.

3 STRUCTURAL ANALYSIS

The structural response to seismic excitation is described by equation of motion

$$\mathbf{M}\ddot{\mathbf{u}} + \mathbf{B}\dot{\mathbf{u}} + \mathbf{K}\mathbf{u} = \mathbf{M}\ddot{\mathbf{u}}_g \tag{13}$$

with the measured ground acceleration vector $\ddot{\mathbf{u}}_g$. Damping is considered through a numerical approach using the velocity-dependent term $\mathbf{B}\dot{\mathbf{u}}$ as well as energy dissipation through inelastic straining and damage evolution. The stiffness of the structure, represented by $\mathbf{K}$, depends on the development of hardening, softening and damage.

3.1 Discretization

Stress-deformation analysis of structures implies the solution of the underlying initial boundary value problem of the body Ω. With the principle of virtual work the weak form of the

equation of motion can be obtained

$$\int_\Omega \delta\mathbf{u}\cdot\rho\ddot{\mathbf{u}}d\Omega+\int_\Omega \delta\mathbf{u}\cdot\mathbf{f}d\Omega+\int_\Omega \delta\boldsymbol{\varepsilon}:\boldsymbol{\sigma}d\Omega= \int_\Omega \delta\mathbf{u}\cdot\mathbf{p}d\Omega+\int_{\partial\Omega}\delta\mathbf{u}\cdot\bar{\mathbf{t}}d\partial\Omega+\int_\Omega\delta\mathbf{u}\cdot\rho\ddot{\mathbf{u}}_\mathbf{g}d\Omega \tag{14}$$

with virtual displacement vector $\delta\mathbf{u}$ and virtual Almansi strain tensor $\delta\boldsymbol{\varepsilon}$, density ρ, acceleration vector $\ddot{\mathbf{u}}$, damping force $\mathbf{f}$, Cauchy stress tensor $\boldsymbol{\sigma}$, volume load vector $\mathbf{p}$, surface load vector $\bar{\mathbf{t}}$. Assuming linear kinematics $\boldsymbol{\varepsilon}=\nabla\mathbf{u}$ and Rayleigh damping $\mathbf{f}_c=\mathbf{c}\dot{\mathbf{u}}$, Equation (14) is discretized in space with the finite-element method, while the Newmark method is used for the discretization in time.
The material behavior is connected to the equation of motion via Cauchy stresses $\boldsymbol{\sigma}$ which are coupled with Almansi strains $\boldsymbol{\varepsilon}$ and internal variables $\mathbf{V}$

$$\boldsymbol{\sigma}=\boldsymbol{\sigma}(\boldsymbol{\varepsilon},\mathbf{V})=\boldsymbol{\sigma}(\boldsymbol{\varepsilon},r,\boldsymbol{\alpha},D) \tag{15}$$

where the latter characterize the state of the material (hardening, softening, damage). The material equations, see Section 2.2, are discretized in time using the implicit Euler approach.

Equation (12) can be assumed to be time-independent since the spatial propagation of the nonlocal damage variable $\bar{D}$ is very fast compared to the evolution of the other variables. The weak form of the additional partial differential equation for the non-local damage field $\bar{D}$ results from weighted residua

$$\int_\Omega\left(\delta\bar{Y}\left(\bar{D}-D\right)-\nabla\delta\bar{Y}\,l_c^2\,\nabla\bar{D}\right)\,d\Omega-l_c^2\int_{\partial\Omega}\delta\bar{Y}\bar{t}_{\bar{D}}\,d\partial\Omega=0 \tag{16}$$

with the virtual nonlocal energy release rate $\delta\bar{Y}$ and Neumann boundary condition $\bar{t}_{\bar{D}}-\mathbf{n}\nabla\bar{D}=0$, which prohibits a damage flux through the boundary of the domain. Here, $\bar{t}_{\bar{D}}$ is forced to zero. The gradient equation is discretized in space by the finite-element method.
Structural analysis is performed using triquadratic twentyseven-node brick elements for the spatial discretization of the field of displacement and the field of damage. The discretization in time uses linear approximations for the material variables while the approximations for the unknowns of the equation of motion depend on the choice of the Newmark integration parameters α and β (see for example [21]). Here, the Newmark integration parameters are set to $\alpha=\frac{1}{2}$ and $\beta=\frac{1}{4}$ which leads to the approach of constant mean acceleration. If damping is considered via Rayleigh damping the parameters $c_\alpha=0.01$ and $c_\beta=0.001$ are employed.

3.2 Global damage index

In order to characterize the damage state of the whole structure a global damage index has to be defined. There exists a large variety of different damage indices from literature and they all agree in having a range between 0 and 1, where 0 corresponds to the undamaged state and 1 to the state of failure [22]. Global damage indices for steel structures are for example proposed by [23, 24, 25], but not all rest on the transformation of damage variables into one global index. Colombo [26], for example, develops an index that takes into account the maximum attained deformation and the energy dissipation in ductile and brittle elements. Ghobarah et al. [27] propose an index which depends on the initial and final stiffness of the structure before and

after the earthquake obtained by push-over analysis. However, if the global damage measure is calculated directly, the local damage distribution remains unknown. In this contribution the indicator for global damage, in the following abbreviated as GDI, is based on the eigenvalue decomposition

$$\left[\mathbf{K}_t - \lambda_{t,i}^2 \mathbf{K}_0\right] \mathbf{v}_{t,i} = \mathbf{0} \tag{17}$$

where $\lambda_{t,i}$ are the eigenvalues, $\mathbf{v}_{t,i}$ are the eigenvectors, $\mathbf{K}_0$ is the initial stiffness matrix and $\mathbf{K}_t$ is the current stiffness matrix due to hardening, softening and damage. Further information concerning this index can be found in [28].

3.3 Seismic excitation of cantilever

In the following the influence on results of structural analysis of different levels of precision concerning the material model is presented for a cantilever consisting of an IPE 80 profile. Moreover the global damage index is evaluated for this structure.

With a height of 5 m and an additional mass of 380 kg assigned to the top the investigated cantilever has an eigenfrequency of 0.55 Hz. The structure is subjected to the north-south component of the Kobe earthquake from 1995 acting in the direction of the strong profile axis, see Figure 6.

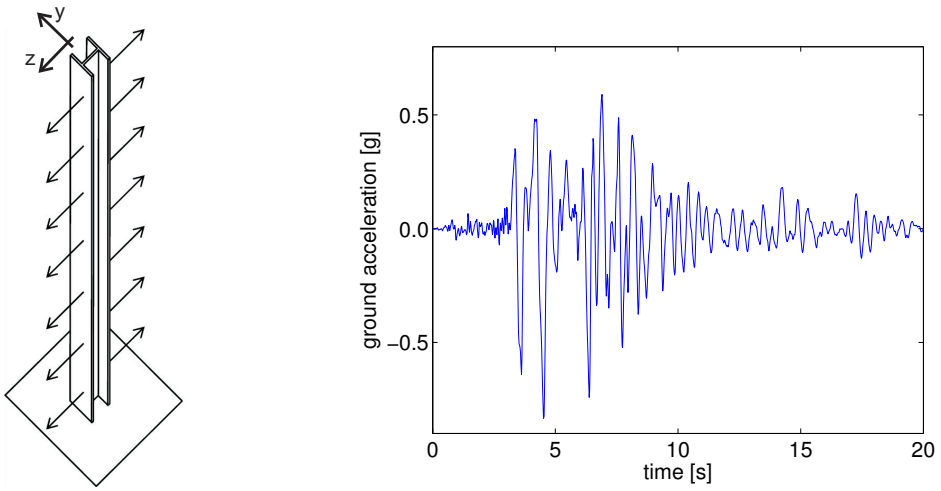

Figure 6: Cantilever and acceleration record of the north-south component of the Kobe earthquake (1995)

In a first analysis elastic material behavior is assumed and damping is neglected. Figure 7(a) depicts the displacement at the top of the cantilever over time. The maximum value of displacement is 69 cm. It is obvious that the vibration mainly consists of the first eigenfrequency. The missing of any damping leads to an increasing displacement even when the amplitudes of the ground acceleration decrease.

For a more detailed simulation the material model is extended by viscoplastic material behavior including isotropic and kinematic hardening. The earthquake causes inelastic cyclic straining in the bottom part of the cantilever. The hystereses in the material behavior lead to dissipation of energy and the top displacement is reduced compared to the elastic behavior. The maximum deflection is 42 cm. Considering the frequencies involved in the vibrations, depicted in the frequency spectra in Figure 7(b), it can be noticed that the amplitude decreases. Furthermore no shift of the involved frequencies can be observed although damping is included by the material model.

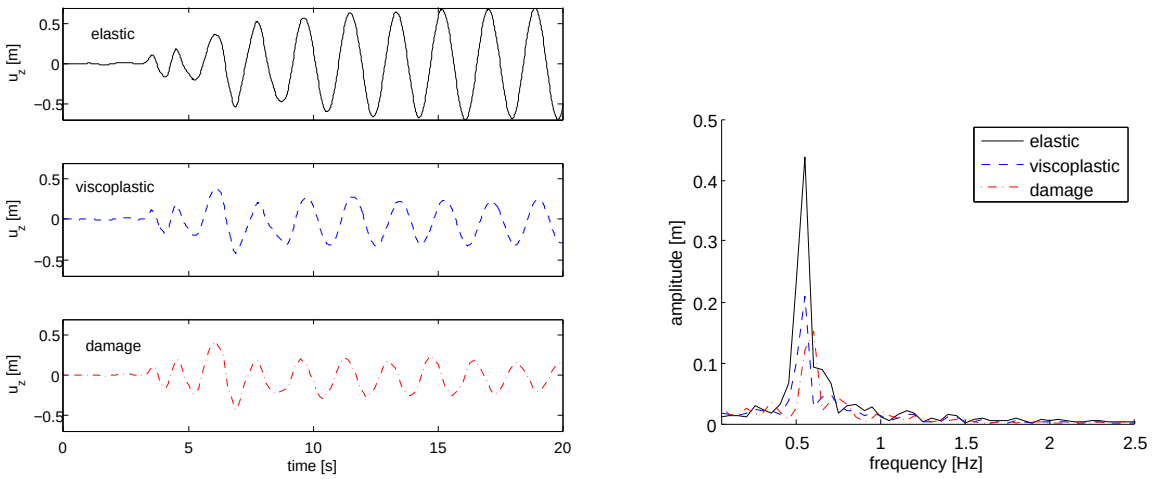

(a) Top displacement (b) Frequency spectra

Figure 7: Displacement of the cantilever top and frequency spectra for elastic, viscoplastic and damaged material

Finally the complete proposed model is applied to compute the response of the cantilever, also considering Rayleigh damping. With about 44 cm the displacement is slightly larger than for the viscoplastic material which is caused by the softening. Because of large inelatic strain material damage evolutes at the base of the cantilever. As an example Figure 8(b) shows the distribution of damage throughout the base of a strongly damaged HEA 180 cantilever. It can be seen that damage occurs in the flanges which are subjected to high alternating tension and compression. Evidently the shear bands accumulate damage and weaken the structure. To evaluate the damage state of the cantilever the global damage index is computed for every timestep, see Figure 8(a). The highest rise of the index corresponds to the largest displacement. With falling intensity of the ground acceleration the damage only increases slightly due to the inelastic deformations remaining below a threshold or only occuring in small exposed regions. The decreasing top displacement is mainly caused by the included numerical damping. The structure shows a slight permanent deformation of 3 cm, since the free vibration does not occur around its zero position.

The deteriorated material at the cantilever base reduces the stiffness of the structure and leads to a shift of the eigenfrequencies which can be seen in the frequency spectrum, see Figure 7(b).

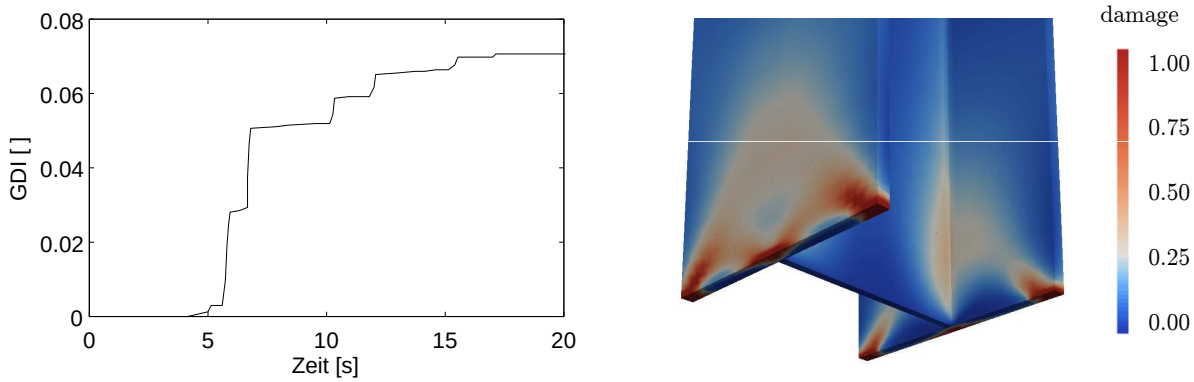

(a) Global damage index

(b) Local damage distribution for HEA 180 base

Figure 8: Damage evolution of the cantilever

4 CONCLUSIONS

Nonlinear time-history computations of structures subjected to earthquakes are possible if material models are used which are able to describe the viscoplastic material behavior. Furthermore the material deterioration has to be taken into account since the softening of the material leads to a shift of the eigenfrequencies and therefore to a different response to the stochastic acceleration.

REFERENCES

[1] J. Chaboche, G. Rousselier, *On the Plastic and Viscoplastic Constitutive Equations - Part I: Rules Developed with Internal Variable Concept*, Journal of Pressure Vessel Technology 105 (1983) 153–158.

[2] J. Chaboche, G. Rousselier, *On the Plastic and Viscoplastic Constitutive Equations - Part II: Application of Internal Variable Concept to the 316 Stainless Steel*, Journal of Pressure Vessel Technology 105 (1983) 159–164.

[3] C. Böttcher, *Geschwindigkeitssensitivität des mechanischen Verhaltens unlegierter Baustähle bei wiederholter Beanspruchung bis in den inelastischen Bereich - experimentelle Untersuchung und Modellierung*. Tech. rep., Fortschrittsbericht VDI Reihe 5, Nr. 654, 2002.

[4] J.L. Chaboche, K. Dang Van, G. Cordier, *Modelization of the strain memory effect on the cyclic hardening of 316 stainless steel*, Transaction of the 5th International Conference on Structural Mechanics in Reactor Technology, Paper No. L11/3, Berlin, Germany, 1979.

[5] H.-J. Scheibe, *Zum zyklischen Materialverhalten von Baustahl und dessen Berücksichtigung in Konstruktionsberechnungen*, Institut für Stahlbau, TU Braunschweig, 1990.

[6] A. Pirondi, N. Bonora, D. Steglich, W. Brocks, D. Hellmann, *Simulation of failure under cyclic plastic loading by damage models*, International Journal of Plasticity 22 (2006) 2146–2170.

[7] M. Alves, *Measurement of ductile material damage*, Mechanics Based Design of Structures and Machines 29 (2001) 451–476.

[8] L. Yang, B. Sun, Y. Guo, *Damage Evaluation Based on Electrical Resistance Measurements*, Key Engineering Materials 385-387 (2008) 589–592.

[9] J. Velde, U. Kowalsky, T. Zümendorf, D. Dinkler, *3D-FE-Analysis of CT-specimens including viscoplastic material behavior and nonlocal damage*, Computational Material Science 46 (2009) 352–357.

[10] S. Krümmling, *Schallemissionsanalyse zum Nachweis der Materialermüdung von Baustahl*, Institut für Stahlbau, TU Braunschweig, 1999.

[11] J. Cordebois, F. Sidoroff, *Damage Induced Elastic Anisotropy*, Proceedings of the Euromech Colloquium 115 (1982) 761–774.

[12] J. Lemaitre, *A Course on Damage Mechanics*, Springer, 1992.

[13] A. Gurson, *Continuum Theory of Ductile Rupture by Void Nucleation and Growth: Part I - Yield Criteria and Flow Rules for Porous Media*, Journal of Engineering Materials and Technology 99 (1977) 2–15.

[14] V. Tvergaard, A. Needleman, *Analysis of the cup-cone fracture in a round tensile bar*, Archives of Mechanics 32 (1984) 157–169.

[15] A. Pirondi, N. Bonora, *Modeling ductile damage under fully reversed cycling*, Computational Material Science 26 (2003) 129–141.

[16] M. Neilson, H. Schreyer, *Bifurcations in Elastic-Damaging Materials*, Damage Mechanics and Localization 142 (1992) 53–67.

[17] Z. Bazant, M. Jirasek, *Nonlocal Integral Formulations of Plasticity and Damage: Survey of Progress*, Journal of Engineering Mechanics 128 (2002) 1119–1149.

[18] M. Jirasek, S. Rolshoven, Regularized Formulations of Strain-Softening Plasticity, D. Kolymbas (Eds.), *Advanced Mathematical and Computational Geomechanics*, Springer, 2003, pp. 269–299.

[19] R. Peerlings, R. de Borst, W. Brekelmans, J. de Vree, *Gradient enhanced damage for quasi-brittle materials*, International Journal for Numerical Methods in Engineering 39 (1996) 3391–3403.

[20] R. Engelen, M. Geers, F. Baaijens, *Nonlocal implicit gradient-enhanced elasto-plasticity for the modelling of softening behavior*, International Journal of Plasticity 19 (2003) 403–433.

[21] K.-J. Bathe, *Finite-Elemente-Methoden*, Springer-Verlag, Berlin, 1990.

[22] A.J. Kappos,*Seismic damage indices for RC buildings*, Progress in Structural Engineering and Materials, 1, 78–87, 1997.

[23] P. Khashaee, *Damage-based Seismic Design of Structures*, Earthquake Spectra, 21, 371–387, 2005.

[24] Z. Shen, A. Wu, *Seismic analysis of steel structures considering damage cumulation*, Front. Archit. Civ. Eng. China, 1, 1–11, 2007.

[25] A. Benavent-Climent, *An energy-based damage model for seismic response of steel structures*, Earthquake Engineering and Structural Dynamics, 36, 1049–1064, 2007.

[26] A. Colombo, P. Negro, *A damage index of generalised applicability*, Engineering Structures, 27, 1164–1174, 2005

[27] A. Ghobarah, H. Abou-Elfath, A. Biddah, *Response-based damage assessment of structures*, Earthquake Engineering and Structural Dynamics, 28, 79–104, 1999.

[28] J. Velde, *3D Nonlocal Damage Modeling for Steel Structures under Earthquake Loading*, Institut für Statik, TU Braunschweig, 2010.